Table 2 Comparison of contributions to Magnus side force coefficient

	C_y (pressure dist.)[6]	C_y (axial shear)	C_y (measured)[6]
Case I	−0.0023	0.0006	−0.0002
Case II	−0.0016	0.0005	−0.0008

metric transition pattern on the nose will contribute significantly to the Magnus moment.

To estimate the significance of this effect for an actual 10° half-angle cone, the contribution due to the pressure field (displacement effect) and axial shear stress are compared using data from Ref. 6. The magnitudes of the calculated terms are shown in Table 2 for two cases: Case I—Mach number = 2, $\alpha = 2$, $Re_L = 5.9 \times 10^6$, $\omega R/V_\infty = 0.24$; and Case II—Mach number = 3, $\alpha = 2$, $Re_L = 4.8 \times 10^6$, $\omega R/V_\infty = 0.19$, along with the measured value of the side force coefficient. The measured transition profiles are shown in Fig. 2.

It can be seen here that the shear contribution is a significant portion of the total and corrects the force in the proper direction for comparison with the measured data but appears to be too small for both cases, especially for Case I. Considering the data uncertainties and the assumptions involved in the shear force calculation, the trend is encouraging.

Thus, it has been shown that the shear contribution to the Magnus force and moment can be significant on nose shapes where a mixed asymmetric boundary layer exists, and a method of estimation indicated.

References

[1] Vaughn, H. R. and Reis, G. E., "A Magnus Theory for Bodies of Revolution," SC-RR-720537, Jan. 1973, Sandia Labs., Albuquerque, N. Mex.

[2] Sedney, R., "Laminar Boundary Layers on a Spinning Cone at Small Angles of Attack in a Supersonic Flow," *Journal of Aeronautical Science*, June 1957, pp. 430–436.

[3] Jacobson, I. D., Vollmer, A. G., and Morton, J. B., "Calculations of the Velocity Profiles of the Incompressible Laminar Boundary Layer on a Yawed Spinning Cone and the Magnus Effect," BRL CR-110, July 1973, Ballistic Research Labs., Aberdeen Proving Ground, Md.

[4] Jacobson, I. D., "Magnus Characteristics of Arbitrary Rotating Bodies," AGARDograph, Dec. 1973.

[5] Monin, A. S. and Yaglon, A. M., "Statistical Fluid Mechanics," *Mechanics of Turbulence*, M.I.T. Press, Cambridge, Mass., 1971.

[6] Sturek, W. B., "Boundary Layer Studies on a Spinning Cone," BRL-1649, May 1973, Ballistic Research Labs., Aberdeen Proving Ground, Md.

Calculation of Low Reynolds Number Flow past a Square Protuberance

CLARENCE W. KITCHENS JR.

Ballistic Research Laboratories, Aberdeen Proving Ground, Md.

Introduction

THE qualitative features of the flowfield downstream of two-dimensional roughness elements immersed in a laminar flat plate boundary layer are well known. Such protuberances are employed in many wind-tunnel experiments to promote transition and assure turbulent boundary-layer characteristics on models. Sedney[1] has described the effects of two- and three-dimensional protuberances on boundary-layer flows. In the two-dimensional case at low speeds, transition generally occurs downstream of the reattachment point if the protuberance height k is considerably less than the undisturbed boundary-layer thickness δ.

This Note describes numerical solutions of the steady-state Navier-Stokes equations for the flowfield near a square two-dimensional protuberance immersed in a plane Couette flow. We expect some of the qualitative features of the separation phenomena induced by the protuberance in the Couette flow to be similar to those found in the flat plate boundary-layer case. Numerical results have been obtained for Reynolds numbers, Re, between 1 and 200 based on plate velocity and protuberance height.

Description of Numerical Calculations

The steady-state Navier-Stokes equations for incompressible flow can be expressed in rectangular coordinates in terms of the vorticity transport equation

$$\frac{\partial}{\partial x}\left(\zeta\frac{\partial\psi}{\partial y}\right)-\frac{\partial}{\partial y}\left(\zeta\frac{\partial\psi}{\partial x}\right)-\nu\left(\frac{\partial^2\zeta}{\partial x^2}+\frac{\partial^2\zeta}{\partial y^2}\right)=0 \tag{1}$$

and a Poisson equation

$$(\partial^2\psi/\partial x^2)+(\partial^2\psi/\partial y^2)+\zeta=0 \tag{2}$$

where vorticity ζ is defined by

$$\zeta=(\partial v/\partial x)-(\partial u/\partial y) \tag{3}$$

and stream function ψ is defined to satisfy the continuity equation

$$u=\partial\psi/\partial y \quad \text{and} \quad v=-\partial\psi/\partial x \tag{4}$$

Numerical solutions of Eqs. (1) and (2) have been obtained using a Gauss-Seidel iteration procedure. The solution technique is based on a method developed by Gosman et al.[2] using an upwind difference scheme to approximate the convective terms.

Figure 1 shows a schematic of the computational region and boundary conditions employed in the numerical calculations. Plate EF moves at constant speed U_o above the stationary plate and protuberance ABCD. Vorticity boundary conditions along the stationary or moving walls are obtained by a Taylor series expansion of the stream function in terms of the mesh spacing normal to the wall ($\Delta\eta$), where ψ_w represents the stream function along the wall and ψ_{w+1}, the value at the grid point adjacent to the wall. Results shown in this Note are based on a second-order accurate equation for the wall vorticity

$$\zeta_w=-\frac{3}{(\Delta\eta)^2}[\psi_{w+1}-\psi_w-(\Delta\eta)U_o]-\frac{\zeta_{w+1}}{2}+0(\Delta\eta^2) \tag{5}$$

which is valid for a stationary wall when U_o is set equal to zero. Calculations were also performed using a first-order accurate equation for wall vorticity with little difference in the results.

Two different grid mesh configurations were used in the calculations. The grid consisted of a 6×11 cell protuberance immersed in a 51×21 cell flowfield for $Re \leqq 50$, with a larger 81×21 cell flowfield used for $Re \geqq 100$. The upstream boundary. AE, was located at approximately $X=-8$ for all Re, where

$$X=(x-x_k)/k \tag{6}$$

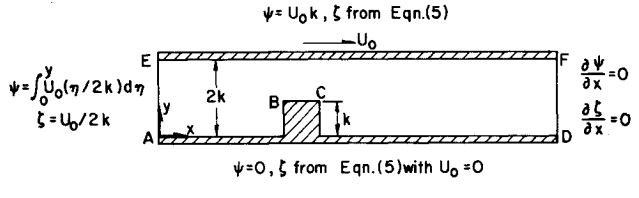

Fig. 1 Schematic of computational region and boundary conditions.

Presented at the Open Forum Session of the AIAA Computational Fluid Dynamics Conference, Palm Springs, Calif., July 19–20, 1973; received January 28, 1974.

Index categories: Boundary-Layer Stability and Transition; Hydrodynamics; Viscous Nonboundary-Layer Flows.

* Aerospace Engineer, Exterior Ballistics Laboratory. Member AIAA.

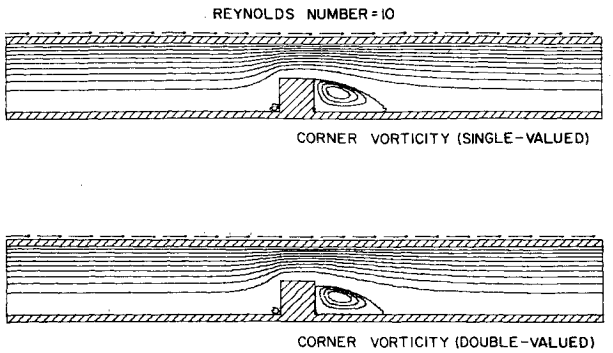

Fig. 2 Streamlines near protuberance for $Re = 10$ based on two different methods for corner vorticity.

refers to distances measured from the position of the protuberance leading edge, x_k, in terms of the protuberance height. The downstream boundary, DF, was located at approximately $X = 9.5$ for $Re \leqq 50$ and at approximately $X = 93.5$ for $Re \geqq 100$.

The specification of vorticity boundary conditions at the sharp protuberance corners, B and C, poses a computational dilemma because more than one method can be used. The two methods used in these calculations show that the predicted location of downstream separation is sensitive to the method employed at low Reynolds numbers. The first method is an attempt to force separation to occur at the downstream corner C. This method treats the corner vorticity as a single-valued function, assuming that the flow along wall BC determines the value of the vorticity at B and C. The second method treats the corner vorticity as a double-valued function, using two different equations depending on whether the corners are considered to be part of the horizontal or vertical protuberance walls. Reference 3 contains details of these methods and a complete description of the numerical results.

Figure 2 illustrates the differences in the solution when these two methods are used to specify the boundary conditions at the sharp protuberance corners. At $Re = 10$, the size of the small upstream separation bubble remains the same independent of the method employed for corner vorticity. The size of the downstream bubble, however, is changed. Separation occurs very close to the downstream corner C using the single-valued method, with reattachment at $X = 3.2$. The double-valued method, on the other hand, predicts separation $(0.1)k$ below corner C with reattachment at $X = 3.0$. At higher Reynolds numbers, separation is predicted less than $(0.1)k$ below the corner with both methods.

The numerical results predict that the flow perturbations introduced by the protuberance persist downstream for long distances and decay more slowly as Re increases. For $Re = 100$ perturbations of the x-component of local velocity no larger than 0.44% of the Couette flow value are present at $X = 93.5$, one cell height off the stationary plate. The flow perturbations are larger for $Re = 200$, 8.1% of the Couette flow value at the same downstream station. Figure 3 shows streamlines in part of the calculated flowfield for $Re = 200$. Separation occurs less than one cell below corner C with reattachment at $X = 26$.

Converged numerical solutions could not be obtained using this iterative procedure for $Re = 300$, 500, and 1000. This is probably caused by the local mesh size and is related to the numerical stability problems encountered by Macagno and Hung.[4] It is also possible, however, that nonconvergence is connected with a physical flow unsteadiness of the type noted by Mueller and O'Leary[5] in two-dimensional backstep experiments for $Re_f > 100$, where Re_f is the Reynolds number based on step height and freestream velocity.

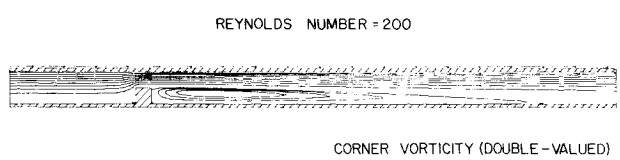

Fig. 3 Streamlines near protuberance for $Re = 200$ based on double-valued method for corner vorticity.

Discussion of Results

Numerical solutions for a square protuberance immersed in a plane Couette flow predict a very small separated flow region upstream of the protuberance, with length and height almost independent of Reynolds number for Re between 1 and 200. The upstream influence of the protuberance does not extend beyond approximately $X = -4$ for all calculated Re. Klebanoff and Tidstrom[6] report upstream influence extending to $X = -30$ for a cylindrical rod in a flat plate boundary layer at Reynolds numbers between 550 and 916 based on protuberance height and freestream velocity. We expect that the upstream separation bubble for a square protuberance in a flat plate boundary layer would be larger than in the present numerical results.

The downstream separation bubble, on the other hand, has a height of order k and a length which increases almost linearly with Re. Figure 4 shows the position of reattachment downstream of the protuberance for all calculated Reynolds numbers. Two sets of experimental data for backstep-type flows are shown for comparison. Measurements by Macagno and Hung[4] for an axisymmetric conduit expansion are plotted against Re_c, based on step height and centerline velocity. The experimental data of Mueller and O'Leary[5] for flow over a two-dimensional backstep are plotted in terms of Re_f. Klebanoff and Tidstrom[6] (not shown in Fig. 4) found reattachment at $30 < X > 40$ for a cylindrical rod in a flat plate boundary layer at Reynolds numbers between 550 and 916.

Results for $Re = 10$ have shown that it is not possible to resolve the exact location of separation on the downstream protuberance face. Numerical results for $Re \geqq 25$ predict separation to occur less than one cell below the downstream corner. Calculations by Mueller and O'Leary[5] for a two-dimensional backstep geometry also predicted separation slightly below the corner, so they investigate the location of separation in their experiments. They remark, "... although suggested in some photographs, separation below the corner could not clearly be seen."

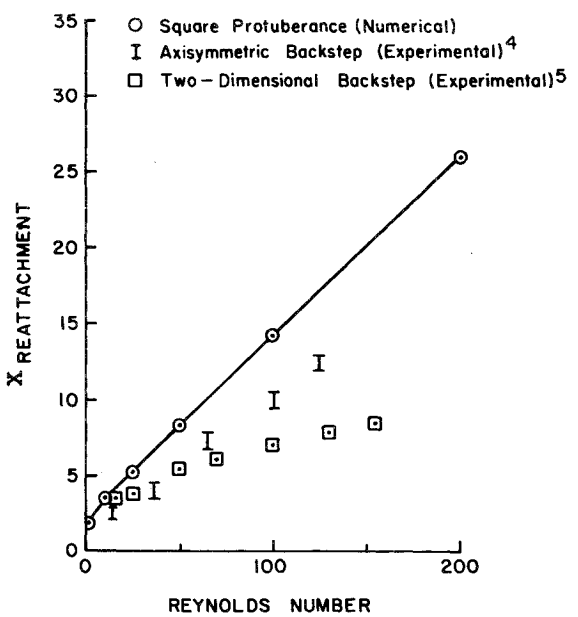

Fig. 4 Variation of downstream reattachment position with Reynolds number.

It thus seems appropriate to interpret our numerical prediction of separation less than one cell below the corner for $Re \geqq 25$ as separation at the corner itself within the accuracy of the finite-difference calculation.

References

[1] Sedney, R., "A Survey of the Effects of Small Protuberances on Boundary-Layer Flows," *AIAA Journal*, Vol. 11, No. 6, June 1973, pp. 782–792.

[2] Gosman, A. D., Pun, W. M., Runchal, A. K., Spalding, D. B., and Wolfshtein, M., *Heat and Mass Transfer in Recirculating Flows*, 1st ed., Academic Press, London, 1969, pp. 94–137.

[3] Kitchens, C. W., Jr., "Separation and Reattachment Near Square Protuberances in Low Reynolds Number Couette Flow," BRL Rept. 1695, Jan. 1974, Ballistic Research Labs., Aberdeen Proving Ground, Md.

[4] Macagno, E. O. and Hung, T. K., "Computational and Experimental Study of Captive Annular Eddy," *Journal of Fluid Mechanics*, Vol. 28, Pt. 1, 1967, pp. 43–64.

[5] Mueller, T. J. and O'Leary, R. A., "Physical and Numerical Experiments in Laminar Incompressible Separating and Reattaching Flows," AIAA Paper 70-763, Los Angeles, Calif., 1970.

[6] Klebanoff, P. S. and Tidstrom, K. D., "Mechanism by which a Two-Dimensional Roughness Element Induces Boundary Layer Transition," *The Physics of Fluids*, Vol. 15, No. 7, July 1972, pp. 1173–1188.

Technical Comments

Further Comments on "Local Nonsimilarity Boundary-Layer Solutions"

DAVID F. ROGERS*
United States Naval Academy, Annapolis, Md.

SPARROW, Quack, and Boerner[1] have developed a new method of solution for nonsimilar boundary layers and presented results for several representative problems. Coxon and Parks[2] commented that Sparrow, Quack, and Boerner neglected a term on the right-hand side of the first auxiliary momentum equation which could be included. Coxon and Parks expressed interest in the effect of retaining this extra term on the accuracy of the results. The results presented below will show that for a particular case the effect is adverse, i.e., the accuracy is decreased. Thus, the closure condition advanced by Sparrow[3] in his reply to Coxon and Parks is to be preferred.

As part of an ongoing study of compressible similar and nonsimilar laminar boundary layers, the effect of this choice of closure condition for Howarth's incompressible retarded flow was investigated. For Howarth's flow, the freestream velocity is given by

$$U(x)/U_\infty = 1-(x/L) \tag{1}$$

Following Ref. 1, the transformations

$$\xi = x/L, \quad \eta = y(U/\nu x)^{1/2}, \quad \psi = (\nu U x)^{1/2} f(\xi,\eta) \tag{2}$$

when applied to the incompressible steady boundary layer equations and no mass transfer boundary conditions, yield

$$f'''+[(\Omega+1)/2]ff''+\Omega(1-f'^2) = \xi(f'g'-f''g) \tag{3}$$

with

$$f(\xi,0)=f'(\xi,0)=0, \quad f'(\xi,\eta\to\infty)\to 1 \tag{4}$$

where

$$\Omega = (x/U)(dU/dx) = \xi/(\xi-1) \tag{5}$$

and the function

$$g(\xi,\eta) = \partial f/\partial\xi \tag{6}$$

The first auxiliary momentum equation for the locally nonsimilar method is obtained by differentiatng Eqs. (3) and (4). This yields

$$g'''+[(\Omega+1)/2][gf''+fg']+(1/2)(d\Omega/d\xi)ff''+(d\Omega/d\xi)(1-f'^2)-2\Omega f'g' = (f'g'-f''g)+\xi(\partial/\partial\xi)(f'g'-f''g) \tag{7}$$

with boundary conditions

$$g(\xi,0)=g'(\xi,0)=0; \quad g'(\xi,\eta\to\infty)\to 0 \tag{8}$$

For the two-equation locally nonsimilar method, the closure condition used in Ref. 1 and recommended in Ref. 3 neglects the entire term $\xi\partial/\partial\xi(f'g'-f''g)$. However, this term may be expanded to yield $\xi(g'^2-g''g)+\xi(f'g'_\xi-f''g_\xi)$. Thus Eq. (1) then may be written as

$$g'''+[(\Omega+1)/2](gf''+fg'')+(1/2)(d\Omega/d\xi)ff''+(d\Omega/d\xi)(1-f'^2)-2\Omega f'g' = (f'g'-f''g)+\xi(g'^2-g''g)+\xi(f'g_\xi'-f''g_\xi) \tag{9}$$

Examination of Eqs. (3) and (9) with boundary conditions given by Eqs. (4) and (8) shows that neglecting only the last term on the right-hand side of Eq. (9) will yield a system of ordinary differential equations at each streamwise location ξ. This is the alternate closure condition discussed by Coxon and Parks.

The effect of the choice of closure condition, i.e., including or not including the term $\xi(g'^2-g''g)$, was investigated by integrating both sets of equations using a fourth-order Runge-Kutta integration scheme with a fixed step size of 0.01.

Table 1 Comparison of closure conditions for the LNS method applied to Howarth flow[a]

ξ	Without term $f''(0)$	$\xi(g'^2-g''g)$ $g''(0)$	With term $f''(0)$	$\xi(g'^2-g''g)$ $g''(0)$
0.0	0.33205754	−1.5429949	0.33205754	−1.5429949
0.01	0.31635425	−1.6254251	0.31656385	−1.6475604
0.02	0.30008091	−1.7167614	0.30122970	−1.7707965
0.03	0.28324570	−1.8185079	0.28679669	−1.9175033
0.04	0.26584963	−1.9324951	0.27463834	−2.0914424
0.05	0.24792076	−2.0609066	0.26688397	−2.2899082
0.06	0.22951139	−2.2063531	0.26560624	−2.4970761
0.07	0.21070638	−2.3719145	0.27115886	−2.6892762
0.075	0.20119169	−2.4633480	0.27605213	−2.7744743
0.076	...	...	0.27716689	−2.7905409
0.08	0.19162534	−2.5612217	No solutions	
0.09	0.17240954	−2.7786882	No solutions	
0.095	0.16278799	−2.8997843	No solutions	
	No solutions			

[a] Numerical results are given to eight significant figures for information purposes only. Results are considered accurate to $\pm 5\times 10^{-6}$. $\eta_{max} = 12.0$ for all calculations.

Received November 5, 1973. Research supported by the Office of Naval Research under P0-4-0071.

Index category: Boundary Layers and Convective Heat Transfer—Laminar.

* Associate Professor, Aerospace Engineering Department. Associate Fellow AIAA.